Influence of Local Orbitals on G_0W_0-bandgap calculations. Example of Magnesium Oxide

BACHELORARBEIT

zur Erlangung des akademischen Grades
Bachelor of Science
(B. Sc.)
im Fach Physik

eingereicht an der
Mathematisch-Naturwissenschaftlichen Fakultät I
Institut für Physik
Humboldt-Universität zu Berlin

von
Herr Christian Vorwerk
geboren am 25.09.1989 in Werl

Betreuung:

1. *Prof. Dr. Dr. hc Claudia Draxl*
2. *Dr. Pasquale Pavone*

eingereicht am: *30.07.2013*

Contents

List of Figures

List of Tables

Chapter 1

Introduction

The electronic structure is a central feature to describe properties of materials. In the last decades, many first-principles calculations of the band structure were performed using Kohn-Sham (KS) density-functional theory (DFT) [7, 10, 3]. However, as the KS eigenvalues have no justification to be considered as single-particle excitation energies, DFT calculations may yield results for the band structure significantly different from experimental values. Especially band gap results are highly imprecise.

The GW approach offers a more direct theoretical method to calculate excitation energies based on many-body Green's functions. Within this framework, the G_0W_0 approximation is commonly used as a perturbative method with DFT calculations as the starting point. Kohn-Sham eigenvalues and eigenvectors are used to calculate more accurate excitation energies. In pseudopotential implementations, this approximation yields semiconductor band gaps in good agreement with experimental results. In the last years, this approach was also implemented in linearized augmented plane wave plus local orbitals ((L)APW+LO) methods [2, 9, 5].

First results (see Ref. [5] and references therein) show that the implementation of G_0W_0 in the (L)APW+LO method underestimates band gaps of semiconductors compared to experimental values as well as to G_0W_0 calculations in the pseudopotential plane-wave method. Insufficient convergence of the results with respect to the number of empty states and the linearization error in the (L)APW+LO method were discussed to be the reason for the shortcomings of the G_0W_0 results. Friedrich and coworkers [4] proposed the usage of local orbitals, that are used successfully to treat semicore states in order to reduce the linearization error of unoccupied states. The attempts have yet lacked a systematic study of the effect of local orbitals depending on the used l-channel, especially for high l-values, and a reproducible choice of reference energies is still missing.

This thesis presents a systematic study of the effect of adding local orbitals for describing unoccupied states in both DFT and G_0W_0 calculations. Local orbitals in l-channels up to $l = 10$ are used and up to 504 local orbitals are added. Two new parameters are introduced, which allow the evaluation of basis-set completeness by convergence with respect to the number of empty states. The scheme is constructed in order to allow reproducibility of the results by only checking convergence within the F-(L)APW method. The influence of local orbitals on groundstate and G_0W_0 band gap calculations is discussed for the example of MgO. The example is chosen as slow convergence with the number of empty states is reported for ZnO [4], similar results are expected for all oxides. MgO also has a similar hybridization as ZnO in the s and p states, which may be a reason for significant linearization errors in

band gap calculations, but with a simple crystal structure which ensures low computational costs. A possible connection between the basis set completeness and the convergence with respect to the number of empty states is analyzed.

Chapter 2

Theoretical Background

2.1 Density Functional Theory

Hohenberg-Kohn Theorem

The basic lemma of Hohenberg and Kohn [7] states that the external potential $v(\mathbf{r})$ is a unique functional of the electron density $n(\mathbf{r})$ of an interacting system of bound electrons. This ensures that the energy of the system can be described as

$$E[n(\mathbf{r})] = \int v(\mathbf{r})\, n(\mathbf{r})\, d\mathbf{r} + F[n(\mathbf{r})]. \tag{2.1}$$

with a potential-independent functional $F[n(\mathbf{r})]$ taking the whole interaction of the electrons into account.

The groundstate of the many-body Schroedinger equation $\hat{H}\,\Psi = E\,\Psi$ can be found by the Rayleigh-Ritz variational method:

$$E = \min_{\tilde{\psi}} \langle \tilde{\Psi} | \hat{H} | \tilde{\Psi} \rangle \tag{2.2}$$

with a normalized trial wavefunction $\tilde{\Psi}$. The Hohenberg-Kohn theorem proves that the minimal principle can be expressed in a trial density $\tilde{n}(\mathbf{r})$ instead of the trial wavefunction. The Rayleigh-Ritz variational method can then be written as

$$E = \min_{\tilde{n}(\mathbf{r})} E[\tilde{n}(\mathbf{r})] = \min_{\tilde{n}(\mathbf{r})} \left\{ \int v(\mathbf{r})\, \tilde{n}(\mathbf{r})\, d\mathbf{r} + F[\tilde{n}(\mathbf{r})] \right\} \tag{2.3}$$

This reduces the calculation of the ground state of the system to the task of minimizing the energy with respect to the three-dimensional electron density. Minimizing the energy under the constraint of constant number of particles means the condition

$$\int \tilde{n}(\mathbf{r})\, d\mathbf{r} = N \quad \Rightarrow \quad \int \delta\tilde{n}(\mathbf{r})\, d\mathbf{r} = 0 \tag{2.4}$$

has to be fulfilled for all trial densities $\tilde{n}(\mathbf{r})$.

Kohn-Sham Equations

For the practical implementation of the Hohenberg-Kohn theorem, one has to know the functional $F[n(\mathbf{r})]$. Kohn and Sham [10] suggested the division of the functional in three terms

$$F[n(\mathbf{r})] = T_s[n(\mathbf{r})] + \frac{1}{2} \iint \frac{n(\mathbf{r})\, n(\mathbf{r}')}{|\mathbf{r} - \mathbf{r}'|}\, d\mathbf{r}\, d\mathbf{r}' + E_{xc}[n(\mathbf{r})] \tag{2.5}$$

where the first term is the kinetic energy $T_s[n(\mathbf{r})]$ of non-interacting electrons, the second term is the Hartree energy, and the third term $E_{xc}[n(\mathbf{r})]$ is the so called exchange-correlation functional, taking into account all interactions between the electrons beyond the Hartree energy. The functional in Eq. (2.5) is stationary under the condition in Eq. (2.4) if the equation

$$\int \delta n(\mathbf{r}) \left[v(\mathbf{r}) + \int \frac{n(\mathbf{r}')}{|\mathbf{r} - \mathbf{r}'|} \, d\mathbf{r}' + \frac{\delta T_s[n(\mathbf{r})]}{\delta n(\mathbf{r})} + \frac{\delta E_{xc}[n(\mathbf{r})]}{\delta n(\mathbf{r})} \right] d\mathbf{r} = 0 \tag{2.6}$$

is fulfilled. Equation (2.6) resembles the one for a non-interacting electron gas in an external potential $V_{eff}(\mathbf{r})$ [10] which is defined as

$$V_{eff}(\mathbf{r}) = v(\mathbf{r}) + \int \frac{n(\mathbf{r}')}{|\mathbf{r} - \mathbf{r}'|} \, d\mathbf{r}' + \frac{\delta E_{xc}[n(\mathbf{r})]}{\delta n(\mathbf{r})} = v(\mathbf{r}) + V^{\text{Hartree}} + V^{\text{xc}}(\mathbf{r}) \tag{2.7}$$

with the Hartree potential V^{Hartree} exchange-correlation potential V^{xc}. By this analogy, the density can be obtained in terms of the solution of the so called Kohn-Sham (KS) equations

$$\left[-\frac{1}{2}\nabla^2 + V_{eff} \right] \psi_{\nu,\mathbf{k}}(\mathbf{r}) = \epsilon_{\nu,\mathbf{k}} \, \psi_{\nu,\mathbf{k}}(\mathbf{r}) \tag{2.8}$$

The wavefunctions $\psi_{\nu,\mathbf{k}}(\mathbf{r})$ are the KS wavefunction of the system. The parameter ν indicates the band index of the wavefunction, $\mathbf{k}$ is the wave vector. From the Kohn-Sham wavefunctions the electron density can be calculated as

$$n(\mathbf{r}) = \sum_{\nu} \sum_{\mathbf{k}} |\psi_{\nu,\mathbf{k}}(\mathbf{r})|^2 \tag{2.9}$$

and the energy as

$$E = \sum_{\nu} \sum_{\mathbf{k}} \epsilon_{\nu,\mathbf{k}} - \frac{1}{2} \iint \frac{n(\mathbf{r}) \, n(\mathbf{r}')}{|\mathbf{r} - \mathbf{r}'|} \, d\mathbf{r} \, d\mathbf{r}' + E_{xc}[n(\mathbf{r})] - \int n(\mathbf{r}) \, \frac{\delta E_{xc}[n(\mathbf{r})]}{\delta n(\mathbf{r})} \, d\mathbf{r} \tag{2.10}$$

Equation (2.8) has to be solved self-consistently since the potential V_{eff} depends on the electron density $n(\mathbf{r})$. For this, the following steps are repeated.

- The Kohn-Sham equations are solved with the effective potential of the previous iteration.
- The electron density is calculated as shown in Eq. (2.9).
- The electron density is used to update the effective potential.

The calculation is started with an initial guess of the electron density and finished when the desired convergence in total energy is reached.

2.2 Green's Function Approach

The quasiparticle energy eigenvalues of an interacting system of bound electrons can be calculated based on the interacting single-particle Green's function $G(\mathbf{r}, \mathbf{r}', \omega)$. Within the Green's function approach, it can be derived [6, 8] that the quasiparticle wavefunctions ϕ_i satisfy the equation

$$\left[-\frac{1}{2}\nabla + V_{ext} + V^{\text{Hartree}} \right] \phi_i(\mathbf{r}) + \int \Sigma(\mathbf{r}, \mathbf{r}', \epsilon_i) \, \phi_i(\mathbf{r}') \, d\mathbf{r}' = \epsilon_i \, \phi_i(\mathbf{r}) \tag{2.11}$$

with the external potential V_{ext}. The self-energy operator $\Sigma(\mathbf{r}, \mathbf{r}', \epsilon_i)$ is a non-hermitian operator taking into account all electron-electron interactions beyond the mean-field approximation.

$\mathbf{G_0W_0}$ Approximation

The G_0W_0 approximation is an approximation of the self energy operator in Eq. (2.11) proposed by Hybertsen and Louie [8]. The Kohn-Sham wavefunctions and energy eigenvalues are assumed to be the zeroth-order approximations of the quasiparticle wavefunctions and energies, respectively. The quasiparticle energies $\omega = \epsilon_{nk}^{\mathrm{qp}}$ can be calculated in a first-order approximation as

$$\epsilon_{\nu,\mathbf{k}}^{\mathrm{qp}} = \epsilon_{\nu,\mathbf{k}} + \langle \psi_{\nu,\mathbf{k}} | \Re[\Sigma(\epsilon_{\nu,\mathbf{k}}^{\mathrm{qp}})] - V^{\mathrm{xc}} | \psi_{\nu,\mathbf{k}} \rangle \tag{2.12}$$

where the self-energy is given in the G_0W_0 approximation by

$$\Sigma(\mathbf{r}, \mathbf{r}', \omega) = \frac{i}{2\pi} \int G_0(\mathbf{r}, \mathbf{r}', \omega + \omega')\, W_0(\mathbf{r}', \mathbf{r}, \omega')\, e^{i\omega'\eta}\, d\omega'. \tag{2.13}$$

The Green's function is approximated by the Green's function of the non-interacting single-particle system, which can be obtained from the Kohn-Sham states by

$$G_0(\mathbf{r}, \mathbf{r}'; \omega) = \sum_{\nu,\mathbf{k}} \frac{\psi_{\nu,\mathbf{k}}(\mathbf{r})\, \psi_{\nu,\mathbf{k}}^*(\mathbf{r}')}{\omega - \epsilon_{\nu,\mathbf{k}} - i\eta(\epsilon_F - \epsilon_{\nu,\mathbf{k}})}. \tag{2.14}$$

Furthermore $W_0(\mathbf{r}, \mathbf{r}', \omega)$ is an approximation for the dynamically screened potential, which is calculated using the dielectric function $\varepsilon(\mathbf{r}, \mathbf{r}'; \omega)$

$$\varepsilon(\mathbf{r}, \mathbf{r}'; \omega) = \delta(\mathbf{r}, \mathbf{r}') - \int v(\mathbf{r}, \mathbf{r}_1)\, P_0(\mathbf{r}_1, \mathbf{r}'; \omega)\, d\mathbf{r}_1 \tag{2.15}$$

with the bare Coulomb potential $v(\mathbf{r}, \mathbf{r}_1) = |\mathbf{r} - \mathbf{r}_1|^{-1}$. The polarizibility $P_0(\mathbf{r}, \mathbf{r}'; \omega)$ in the random phase-approximation (RPA) is calculated as

$$P_0(\mathbf{r}, \mathbf{r}'; \omega) = -\frac{i}{2\pi} \int G_0(\mathbf{r}, \mathbf{r}'; \omega + \omega')\, G_0(\mathbf{r}', \mathbf{r}; \omega')\, e^{i\omega'\eta}\, d\omega'. \tag{2.16}$$

The screened potential $W_0(\mathbf{r}, \mathbf{r}', \omega)$ is then calculated as

$$W_0(\mathbf{r}, \mathbf{r}', \omega) = \int \varepsilon^{-1}(\mathbf{r}, \mathbf{r_1}; \omega)\, v(\mathbf{r}_1, \mathbf{r}')\, d\mathbf{r}_1. \tag{2.17}$$

It is common to divide the self-energy operator into correlation and exchange parts by defining

$$W_0^c(\mathbf{r}, \mathbf{r}'; \omega) = W_0(\mathbf{r}, \mathbf{r}'; \omega) - v(\mathbf{r}, \mathbf{r}') \tag{2.18}$$

which yields the self-energy operator $\Sigma(\mathbf{r}, \mathbf{r}'; \omega)$ as the sum of correlation and exchange self energy:

$$\Sigma(\mathbf{r}, \mathbf{r}'; \omega) = \Sigma^x(\mathbf{r}, \mathbf{r}') + \Sigma^c(\mathbf{r}, \mathbf{r}'; \omega) \tag{2.19}$$

Chapter 3

Methodology

3.1 Basis Sets

Density functional calculations are implemented using the Ritz-Rayleigh variational principle. The Kohn-Sham wavefunctions $\psi_{\nu,\mathbf{k}}(\mathbf{r})$ are expressed as a linear combination of basis functions $\phi^i_{\mathbf{k}}(\mathbf{r})$:

$$\psi_{\nu,\mathbf{k}}(\mathbf{r}) = \sum_i c^i_{\nu,\mathbf{k}}\, \phi^i_{\mathbf{k}}(\mathbf{r}). \tag{3.1}$$

This transforms the Kohn-Sham equations (2.8) into a set of algebraic equations, which can be written as a matrix equation

$$\left[\tilde{\mathbf{H}}(\mathbf{k}) - \epsilon_{\nu,\mathbf{k}}\tilde{\mathbf{S}}(\mathbf{k})\right] \cdot \tilde{\mathbf{c}}_{\nu,\mathbf{k}} = 0 \tag{3.2}$$

with the Hamiltonian matrix $\tilde{\mathbf{H}}(\mathbf{k})$ defined as

$$\tilde{H}^{j,i}(\mathbf{k}) = \int_\Omega \left[\phi^j_{\mathbf{k}}(\mathbf{r})\right]^* \left[-\frac{1}{2}\nabla^2 + V_{eff}\right] \phi^i_{\mathbf{k}}(\mathbf{r})\, d\mathbf{r} \tag{3.3}$$

with the unit cell volume Ω, and the overlap matrix $\tilde{\mathbf{S}}(\mathbf{k})$ as

$$\tilde{S}^{j,i}(\mathbf{k}) = \int_\Omega \left[\phi^j_{\mathbf{k}}(\mathbf{r})\right]^* \phi^i_{\mathbf{k}}(\mathbf{r})\, d\mathbf{r}\ . \tag{3.4}$$

For a given wavevector $\mathbf{k}$, $\tilde{\mathbf{c}}_{\nu,\mathbf{k}}$ is a vector in i, its length is equal to the number of basis functions. Furthermore $\tilde{\mathbf{H}}(\mathbf{k})$ and $\tilde{\mathbf{S}}(\mathbf{k})$ are $M \times M$ quadratic matrices with M equal to the number of basis functions.

If a complete, usually infinite basis set is used, the wavefunction can be expressed exactly. As in numerical implementations only basis sets with a limited number of basis functions can be used, the choice of an appropriate basis set can reduce the number of basis functions and therefore also the computational cost of the calculation.

3.1.1 Plane-Wave Basis Set

Due to the translational symmetry of a crystal, plane waves are a convenient basis set in solids:

$$\psi_{\nu,\mathbf{k}}(\mathbf{r}) = \frac{1}{\sqrt{\Omega}} \sum_{|\mathbf{k}+\mathbf{G}|<K_{max}} c^{\mathbf{G}}_{\nu,\mathbf{k}} \exp\left[i(\mathbf{k}+\mathbf{G})\cdot\mathbf{r}\right] \tag{3.5}$$

Plane waves as basis functions have some useful properties for the implementation: These basis functions are orthogonal and the overlap matrix is diagonal. Furthermore, functions can also be handled easily in reciprocal space.

However, a plane-wave basis is problematic fir treating the strongly varying wavefunction close to the atomic nuclei due to the singularities of the crystal potential. In this region an extremely high number of plane wave is needed to describe the wavefunction, resulting in very high K_{max} values needed for converged results. For that reason plane-wave basis can only be used with smoothed pseudo potentials. The main idea behind pseudo potentials is that only valence states participate in the bonding process. So the electrostatic potential of the nucleus and the core electrons are combined in a potential which is smoother than the actual all-electron potential. This formalism yields correct wavefunctions between atomic positions and approximates the wavefunctions close to the nuclei.

3.1.2 Augmented Plane-Wave Method

Augmented plane-wave (APW) basis sets [16, 1] take a different approach to the strong oscillations of the wavefunction close to the atomic positions. The unit cell of the crystal is divided into two different areas: The "Muffin-Tin"(MT) spheres are non-overlapping spheres centered at the atomic positions. The interstitial region (IR) is the space between the spheres.

The basis functions of the APW method have the following form:

$$\phi_{\mathbf{G}}(\mathbf{k},\mathbf{r}) = \begin{cases} \frac{1}{\sqrt{\Omega}} \exp\left[i(\mathbf{k}+\mathbf{G})\cdot\mathbf{r}\right] & \mathbf{r} \in \mathrm{IR} \\ \sum_{l,m} A_{l,m}^{\mathbf{G}}(\mathbf{k})\, u_l(x_s,\epsilon)\, Y_{l,m}(\hat{\mathbf{x}}_s) & \mathbf{r} \in \mathrm{MT}(\mathbf{r}_\mathrm{s}) \end{cases} \tag{3.6}$$

Ω is the unit cell volume, $Y_{l,m}$ is the spherical harmonic, $\mathbf{x}_s = \mathbf{r} - \mathbf{r}_s$, and $\mathrm{MT}(\mathbf{r}_\mathrm{s})$ is the muffin-tin sphere centered at the atomic position $\mathbf{r}_s$. The radial functions $u_l(r,\epsilon)$ are the solutions of the radial Schroedinger equation

$$\left(-\frac{1}{2}\frac{\partial^2}{\partial r^2} + \frac{1}{2}\frac{l(l+1)}{r^2} + V(r) - \epsilon\right) r\, u_l(r) = 0 \tag{3.7}$$

with the spherical averaged potential $V(r)$ in the muffin-tin sphere. The coefficients $A_{l,m}^{\mathbf{G}}(\mathbf{k})$ in Eq. (3.6) are not variational coefficients but are determined by the continuity condition of the basis functions at the sphere boundaries.

Most implementations of APW basis sets use the so called shape approximation: The crystal potential is constant in the interstitial space and spherically averaged in the MT spheres.

The major drawback of the APW method is that since the basis functions inside the MT spheres depend on the energy eigenvalues $\epsilon_{\nu,\mathbf{k}}$, Eq. (3.2), becomes a nonlinear eigenvalue problem. This changes the numerical solution of the algebraic Eq. (3.2). If the eigenvalue problem in Eq. (3.2) were linear, one diagonalization for every $\mathbf{k}$-point had to be performed in order to find all eigenvalues $\epsilon_{\nu,\mathbf{k}}$. As in the APW basis set matrices depend on energy eigenvalues, the equation has to be evaluated for each eigenvalue ϵ, making the calculation significantly more time-consuming. Another computational drawback of the APW method is the fact that in general there are reference energies for which the radial function vanishes at the sphere boundary. In this case, the augmentation of the radial functions with the plane waves in the interstitial area is not possible. This is called the asymptote problem [14].

3.1.3 Linearized Augmented Plane-Wave Method

All above mentioned difficulties of the APW method are overcome in the linearized augmented plane-wave (LAPW) method. The LAPW basis set linearizes the eigenvalue problem of the APW basis by expanding the radial function $u_l(r,\epsilon)$ of equation (3.7) in a Taylor series around a l-dependent reference energy ϵ_l terminated after the linear term

$$u_l(r,\epsilon_{\nu,k}) = u_l(r,\epsilon_l) + (\epsilon_{\nu,k} - \epsilon_l)\,\dot{u}_l(\epsilon_l) + ... \tag{3.8}$$

The usage of reference energies, also called linearization energies, ensures the energy-independence of the basis. As the error in the wavefunction is in the second order by variational methods, it can be shown that the error in the eigenvalues, called linearization error, is in the fourth order. Linearization energies are chosen to be close to the energy eigenvalues to increase the accuracy. Usually the reference energy is set to the center of gravity of the valence band with the respective l-character. This leads to the basis set

$$\phi_{\mathbf{G}}(\mathbf{k},\mathbf{r}) = \begin{cases} \frac{1}{\sqrt{\Omega}} \exp\left[i(\mathbf{k}+\mathbf{G})\cdot\mathbf{r}\right] & \mathbf{r} \in \mathrm{IR} \\ \sum_{l,m}\left[A^{\mathbf{G}}_{l,m}(\mathbf{k})\,u_l(x_s,\epsilon_l) + B^{\mathbf{G}}_{l,m}(\mathbf{k})\,\dot{u}_l(x_s,\epsilon_l)\right] Y_{l,m}(\hat{\mathbf{x}}_s) & \mathbf{r} \in \mathrm{MT}(\mathbf{r}_\mathrm{s}) \end{cases} \tag{3.9}$$

The coefficients $A^{\mathbf{G}}_{l,m}(\mathbf{k})$ and $B^{\mathbf{G}}_{l,m}(\mathbf{k})$ are determined by the continuity of the wavefunction and its slope at the sphere boundaries.

The LAPW method linearizes the eigenvalue problem of the APW basis set. Thus, it is computationally much less demanding. The asymptote problem does also not occur using LAPW, as in general if the radial function u_l vanishes at the sphere boundary, neither the first derivative of the radial function nor the derivative with respect to the energy vanish. For this reason, even in these cases the augmentation is unproblematic. Because of the additional constraint to calculate the coefficient $B^{\mathbf{G}}_{l,m}(\mathbf{k})$ the basis set is stiffer than the APW basis set, meaning that the converge of results with respect to K_{max} is slower [14].

3.1.4 Concept of Local Orbitals

Semicore States

The application of the LAPW method becomes problematic if states with the same l-value but considerably different energies need to be considered at the same time. This is easy to realize since the reference energy ϵ_l does not depend on the principle quantum number n.

This problem was first encountered in the treatment of semicore states. It can be shown that in the LAPW method the basis functions within the MT spheres are orthogonal to all core states which are completely confined within the MT sphere. Semicore states are core states that are extended beyond the sphere boundary. If the linearization energies are set in the valence region, groundstate results can be obtained with high accuracy but semicore states are not described because of the significant linearization error. If the linearization energies are decreased to reduce the linearization error of the semicore eigenvalues, the valence states get highly inaccurate. To treat this states more accurately the addition of local orbitals (LO) was developed.[13]

These local orbitals are function completely contained within the MT spheres, they vanish in function and slope at the sphere boundaries. In the LAPW+LO basis they have the following form

$$\phi_{LO}(\mathbf{r}) = \Big[A_{LO}\, u_l(r,\epsilon_l) + B_{LO}\, \dot{u}_l(r,\epsilon_l) + C_{LO}\, u_l(r,\epsilon_l^{(2)})\Big]\, Y_{l,m}(\hat{\mathbf{r}}) \tag{3.10}$$

where $\mathbf{r}$ is coordinate to the atomic position. The local orbitals consist of radial functions evaluated at two different reference energies ϵ_l and $\epsilon_l^{(2)}$. The first energy is commonly chosen the one of the corresponding valence state, the second can be set to a different energy region, for example semicore states or unoccupied states. The determination of the three coefficients A_{LO}, B_{LO} and C_{LO} relies on the condition that the value and slope of the LO vanish at the sphere boundaries and that the function is normalized are used. The indices l and m are omitted in equation (3.10) for clarity. The LAPW+LO basis set adds more variational freedom to the LAPW method without adding new boundary conditions. It is reported to have the same convergence with respect to K_{max} as the LAPW method as it has the same number of sphere boundary conditions [15].

The LAPW+LO method is a popular choice of basis set in solid state DFT calculations because it offers high precision results with reasonable computational effort [9, 15].

APW+lo Method

To combine the linear eigenvalue problem of the LAPW+LO method and the fast convergence of the APW method with respect to K_{max}, Sjörsted and coworkers developed the APW+lo method [15]. It uses the basis functions described in equation (3.10) but evaluated at reference energies ϵ_l instead of the band energies ϵ. Unlike LAPW, which reduces the linearization error by adding the energy derivative of the radial function, only local orbitals are used. The local orbitals in this methods have the following form

$$\phi_{lo}(\mathbf{r}) = \left[A_{lo}\, u_l(r,\epsilon_{lo}) + B_{lo}\, \dot{u}_l(r,\epsilon_{lo})\right] Y_{l,m}(\hat{\mathbf{r}}) \tag{3.11}$$

The gold standard for all-electron DFT calculations in the last years have been calculations with the FP-(L)APW+lo method. This method uses the APW+lo basis for low l-values which usually are slow-converging and LAPW+LO for all other l-values. The basis also lifts the shape approximation of the original APW method.

Chapter 4

Practical Approach

4.1 MgO in Rocksalt Structure

All calculations are performed assuming the rocksalt structure, which is found to be the most common crystal structure of MgO [11]. The lattice constant was obtained by calculating the total energy using the PBEsol functional [12] for different lattice constants.The equilibrium unit-cell volume can be obtained by minimizing the total energy, as it is shown in Figure (4.1). The lattice constant is not converged with respect to the numerical parameters, as a complete and careful calculation of the lattice parameter is not the topic of this thesis.

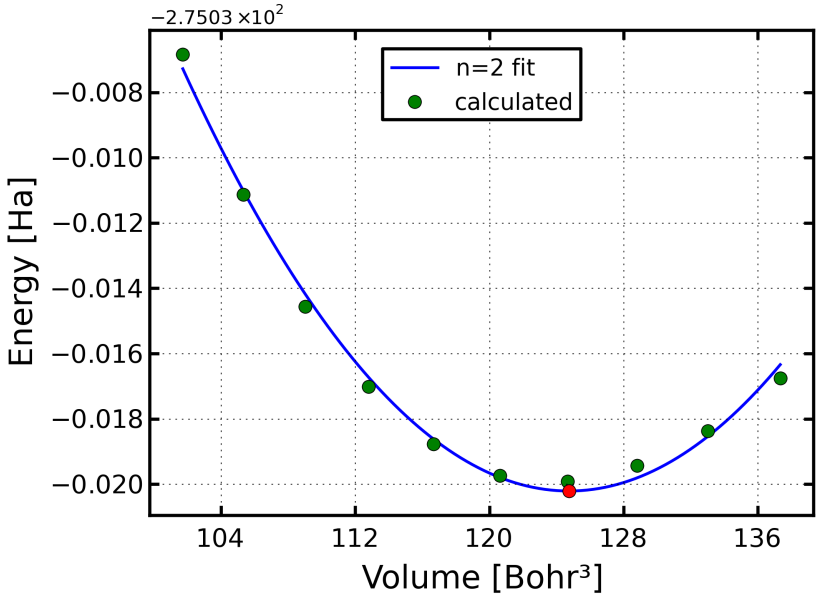

Figure 4.1: *Dependence of the total energy on the volume of the unit cell. The calculations are shown with a polynomial fit of order 2.*

The resulting lattice constant is $a = 3.9658$ Bohr $= 2.0986$ Å. Figure (4.2) shows the crystal structure.

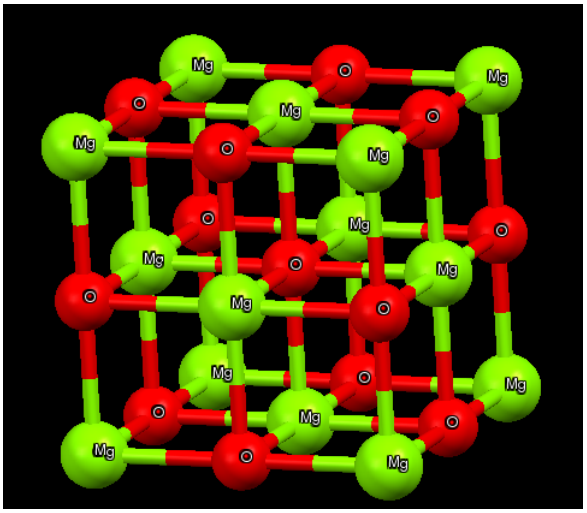

Figure 4.2: *Visualization of crystal structure of MgO*

4.2 Numerical Parameters

DFT

Ground-state calculations are performed on a 4×4×4 **k**-points grid. Taking symmetry into account, calculations in **k**-space are performed using 8 **k**-points. The value of $K_{\max} \cdot R_{\mathrm{MT,max}} = 8$ is chosen, resulting in $K_{\max} = 5.52$ Bohr^{-1}. The radius of the MT spheres is 2.0 Bohr for Mg and 1.45 Bohr for O.

To solve the radial Schroedinger equation within the MT sphere of O atoms a number of 138 radial points is sufficient, for Mg atoms the number has to be increased to 500 to accurately describe the highly varying radial functions of local orbitals with high l-values.
For all DFT calculations the PBESol functional is chosen [12].

In all calculations the (L)APW+LO method was used: For both elements $l = 0$ and $l = 1$ states are described by the APW+lo method, all states with $l > 1$ with the LAPW+LO method.

In the following chapter 'default description' denotes the default choice basis set in the `exciting` code [2]. For O atoms the default description means that no local orbitals are added beyond the (L)APW+LO method. For Magnesium atoms 4 local orbitals are added in the default description. One $l = 0$ LAPW local orbital and three $l = 1$ LAPW local orbitals are added at energies below the Fermi level to describe semicore states. These local orbitals are not changed during the following calculations, as the the description of occupied states is not in the scope of this thesis.

G_0W_0

G_0W_0-calculations were performed on different **q**-points grids. Integrations along the frequency axis were performed using 32 imaginary frequency points [9]. The mixed product basis parameters have been chosen to have the values $l_{max}^{\mathrm{MB}} = 3$ for the MT region and $Q = 1$ for the interstitial region [9], but convergence with respect to the parameter l_{max}^{MB} is tested. For the initial groundstate calculations the chosen parameters are the one mentioned in the previous paragraph.

4.3 Treatment of Unoccupied States

A systematic treatment of high-lying unoccupied states in DFT calculations requires new definitions for convergence criteria and a systematic approach to describe this states with local orbitals.

To describe basis-set completeness in the unoccupied energy region in terms of convergence, two new parameters are introduced: a cut-off energy E_c and a maximal l-value l_{max}, which defines the highest l-value up to which local orbitals are added, starting from $l = 0$. Local orbitals are added at reference energies which are chosen as the eigenvalues of a model Hamiltonian describing a particle in a spherical symmetric box with zero potential inside and infinitive potential outside the box. As solutions of this Hamiltonians vanish at the sphere boundary, they have the same boundary conditions as the APW local orbital and can be interpreted as the zeroth-order approximation to the local orbitals. The reference energies can then be calculated analytically as

$$\epsilon_{n,l} = \frac{b_{n,l}^2}{2R_{\mathrm{MT}}^2} \tag{4.1}$$

where $b_{n,l}$ as n-th zero point of the spherical Bessel function j_l and R_{MT} is the radius of the MT sphere. Reference energies can be chosen arbitrarily but have to ensure that the resulting radial functions of the local orbitals are not linear dependent. This approximation yields reference energies such that local orbitals are not linear dependent in a wide energy range up to 90 Hartree above the Fermi level.

The cut-off energy E_c defines the highest reference energy as

$$E_c \geq \epsilon_{n,l} \quad \forall\, n, l \tag{4.2}$$

Defined as this, E_c specifies the number of local orbitals used in each l-channel. The number of local orbitals for a value of E_c depend on the radius of the MT sphere of the element. For an arbitrary value for E_c more local orbitals are added to Mg atoms compared to O atoms.

It is known that G_0W_0-calculations are dependent on a careful convergence with respect to the number of empty states and, in some cases, need a high number of empty states to reach convergence. In this thesis, local orbitals with l-values up to $l = 10$ were used and their impact analyzed as well as cut-off energies up to $E_c = 90$ Ha to describe states beyond 20 Ha above the Fermi level.

Chapter 5

Results

5.1 Unoccupied States in Groundstate Calculations

5.1.1 Density of States

To evaluate the dependence of the total density of states (TDOS) on the inclusion of local orbitals, calculations were performed with one of the constituent elements of MgO in the default description and different cut-off energy and maximal l-value for the other element. Density of states calculations were compared to reference ones where a high cut-off energy and maximal l-value were used. As one could set the reference calculations to arbitrary values of l_{max} and E_c, the definition of the reference calculations determines the energy range in which the influence of local orbitals is analyzed. Reference energies defined in this thesis allow an evaluation of an energy region up to around 29 Ha above the Fermi level and permit an addition of up to 504 local orbitals in all l-channels up to $l = 10$.

The converged energy region is defined as the region in which the difference in the total density of states for every energy point is smaller than $\Delta_{TDOS} = \pm 0.2$ Ha^{-1}a$_0^{-3}$.

Using the results of converging the TDOS for each element, convergence behavior with addition of local orbitals for both elements is analyzed and discussed. In this context, an optimized scheme of adding local orbitals is presented in order to reduce the number of local orbitals needed.

Convergence for each element

For Mg atoms the reference calculation has a cut-off energy $E_c = 70$ Ha and $l_{max} = 10$, resulting in a total number of 504 local orbitals. For O atoms a cut-off energy $E_c = 90$ Ha and $l_{max} = 10$ has been chosen, resulting in 341 local orbitals.

The distribution of local orbitals for these references is displayed in Table (5.1).

l	# local orbitals for Mg	# local orbitals for O
0	8	6
1	24	15
2	30	25
3	42	28
4	45	36
5	55	33
6	52	39
7	60	45
8	68	34
9	57	38
10	63	42
total	504	341

Table 5.1: *Distribution of local orbitals for reference calculations for each element*

The density of states with lower l_{max} and cut-off energy were compared against this reference. An example can be seen in Fig. (5.1).

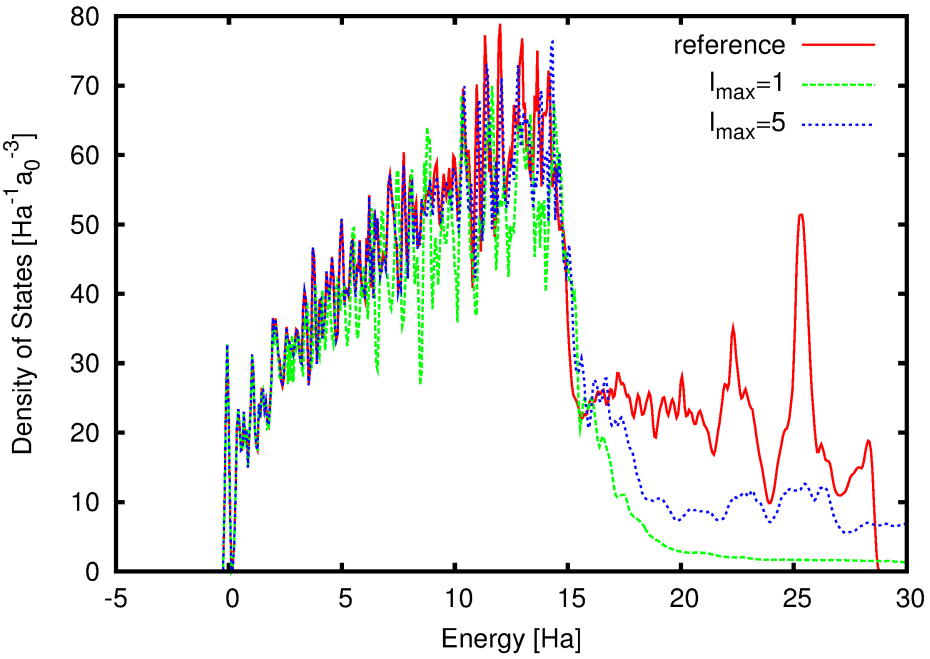

Figure 5.1: *TDOS for the reference calculation and calculation with lower l_{max} values(1 and 5). For all calculations the same cut-off energy of 70 Ha is chosen. Local orbitals are only added for Mg atoms*

Results in Fig. (5.1) show that the density of states of all three calculations is identical for the occupied states below Fermi level and for the low energy unoccupied states. However, large differences are found in the high-energy unoccupied region. The difference between the results is smaller for calculations with a smaller difference in l_{max}.

TDOS calculations were performed for cut-off energies between 5 and 70 Ha for the Mg atoms and 10 to 90 Ha for the O atoms using local orbitals up to $l_{max} = 10$.

For each l_{max} and E_c the converged energy region, as defined above, is calculated. The converged energy regions are shown in Fig. (5.2) and (5.3).

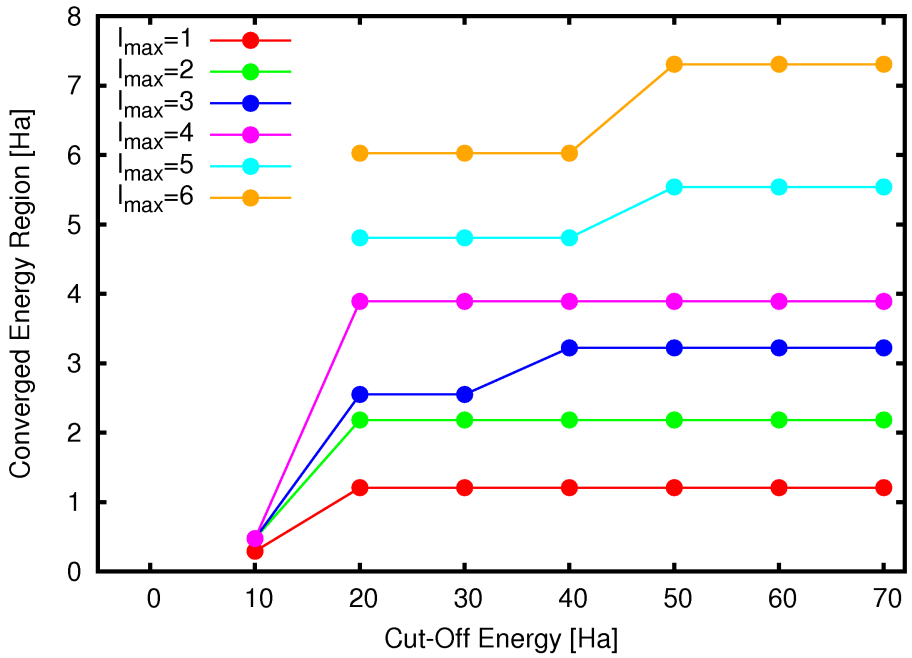

Figure 5.2: *Dependence of the converged energy region on the cut-off energy for Mg. For each calculated cut-off energy the total number of local orbitals is shown. Lines are inserted to guide the eye.*

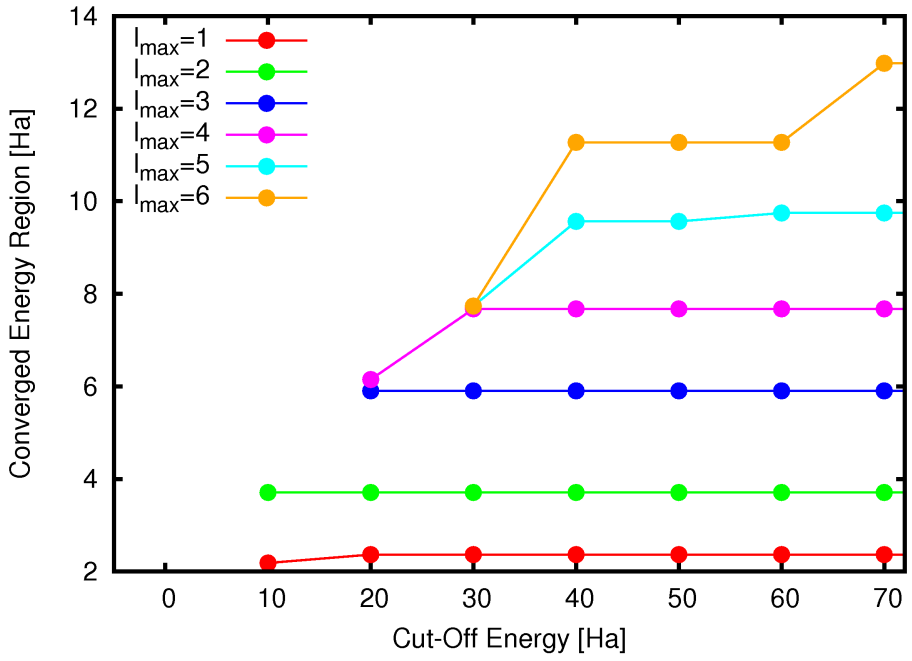

Figure 5.3: *Dependence of the converged energy region on the cut-off energy for O. For each calculated cut-off energy the total number of local orbitals is shown. Lines are inserted to guide the eye.*

The converged energy region is increasing with an increase of l-channels used for both elements. The addition of local orbitals in the MT spheres of oxygen yields higher converged energy ranges than the addition in the ones of Mg. Already the addition of 2 s local orbitals and 6 p local orbitals for oxygen increases the converged region to 3.709 Ha, whereas even a high amount of s and p local orbitals for magnesium is not sufficient to reach converged energy regions beyond 2.367 Ha. For all l-channels the same amount of local orbitals yields larger converged energy regions for oxygen than for magnesium.

In theory one expects that with the addition of local orbitals with higher reference energies the converged region increases, since the linearization error for the unoccupied states with increasing energy is reduced. As it can be seen in Fig. (5.2) and (5.3) this is only valid in a small energy region for both elements. If more local orbitals with higher reference energies are added, the converged energy region does not increase. High energy states cannot be described with s-,p- or d-states in the MT sphere, their description has to involve the usage of radial functions in much higher l-channels. Because the radial functions of different l-channels are diagonal to each other, the linearization error of states described by high l-channels cannot be corrected by local orbitals in much lower l-channels. To describe higher energy regions additional l-channels have to be involved and a addition of local orbitals in low l-channels is not sufficient.

Convergence for both elements combined

Using the results displayed in Fig. (5.2) and (5.3) an optimized amount of local orbitals is used in all further groundstate calculations. The minimal amount of local orbitals and the minimal reference energies needed to yield the maximal converged energy range are used, in order to obtain an accurate but efficient description of the unoccupied states. The number of local orbitals in this optimized scheme is displayed in table (5.2).

The number of local orbitals needed is significantly smaller in every l-channel for the oxygen than for the magnesium atoms as it is described above.

l	# local orbitals for Mg	# local orbitals for O
0	5	2
1	12	6
2	15	10
3	28	7
4	36	9
5	55	33
6	39	26
7	60	45
8	68	34
9	57	38
10	63	42

Table 5.2: *Distribution of local orbitals for optimized combined calculations*

Using this combination of local orbitals the converged energy region can be calculated depending on the l_{max}, as displayed in Fig. (5.4). The converged energy region is increasing approximately linearly with the increase of l-channels included.

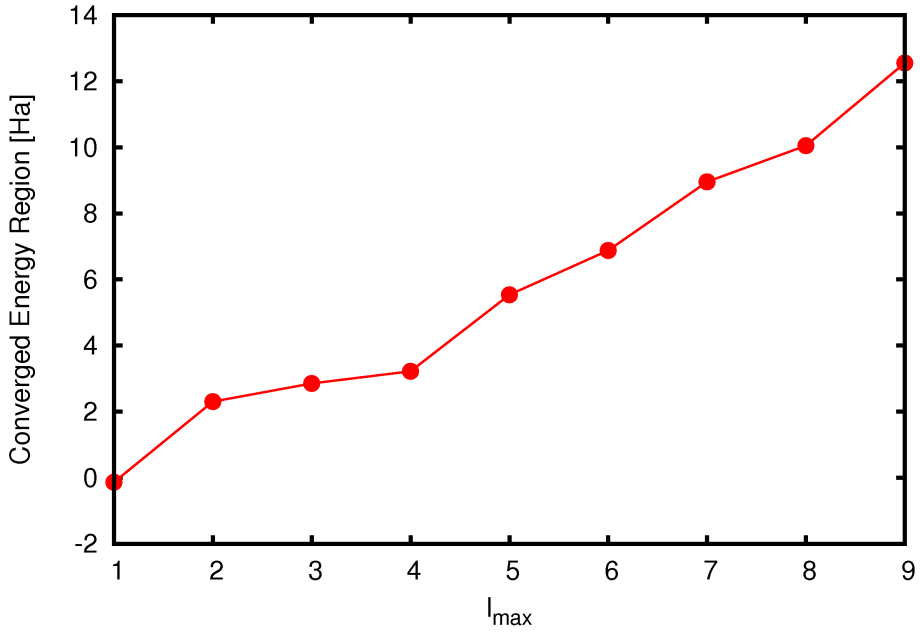

Figure 5.4: *Dependence of the converged energy region on l_{max}. The converged energy region is increasing linearly with the addition of more l-channels. The line is included to guide the eye.*

5.1.2 Kohn-Sham Eigenvalues

In addition to the total density of states, the energy eigenvalues themselves can be used to show that the usage of local orbitals gives a better description of the unoccupied energy region. Similar to Friedrich and coworkers [5] the deviation of the energy eigenvalues of calculations with low l_{max} in the optimized combined description to the reference calculation at the Γ point in **k**-space are shown in Fig. (5.5).

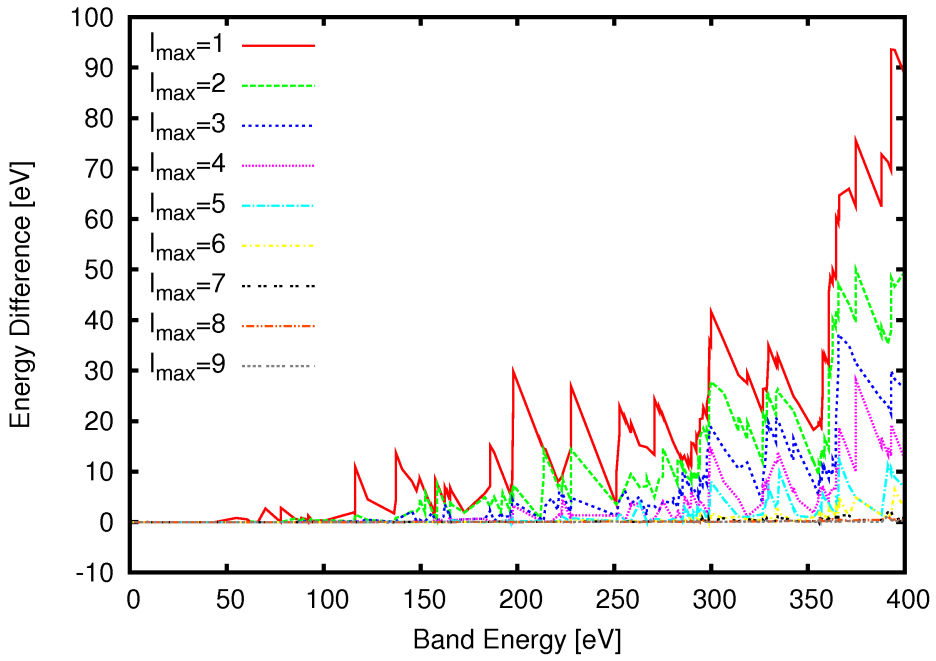

Figure 5.5: *Deviation of energy eigenvalues with different l_{max} to the reference calculation at Γ-point.*

Figure (5.5) shows the same features already seen in the convergence of the density of states: The difference in eigenvalues is increasing with the energy, as high-energy states are described worse than low lying unoccupied and occupied states. The deviation is decreasing with the addition of local orbitals with higher l_{max}-values. High-energy states can only be described accurately when high l_{max}-values well beyond 3 or 4 are included.

In the converged energy region as displayed in Fig. (5.4) the deviation to the reference calculations is smaller than 0.3 eV for all l_{max}. This shows that an evaluation of the density of states or the energy eigenvalues leads to similar results. As the deviation below the Fermi level is negligible the total energy is not changed by the addition of local orbitals. The local orbitals just give a more accurate description of the unoccupied states, especially at high energy, which do not contribute to the total energy.

5.2 Unoccupied States in G_0W_0 Calculations

5.2.1 Convergence Study of the Band Gap

Convergence with the number of empty states

Band-gap calculations were performed on a 2×2×2 , 4×4×4 and 6×6×6 **q**-points grid, with different l_{max}-values for local orbitals and a range of empty states up to 480. The convergence of the band gap with respect to the number of empty states is difficult, as it had been shown for ZnO [4]. Additional to the analysis of the band gap itself, the contributions to the self energy of the valence band maximum (VBM) and the conduction band minimum (CBM) are evaluated. All G_0W_0 calculation yield a direct band gap at the Γ point in **k**-space.

The dependence of the band gap on the number of empty states on the 2×2×2 **q**-points grid is displayed in Fig. (5.6).

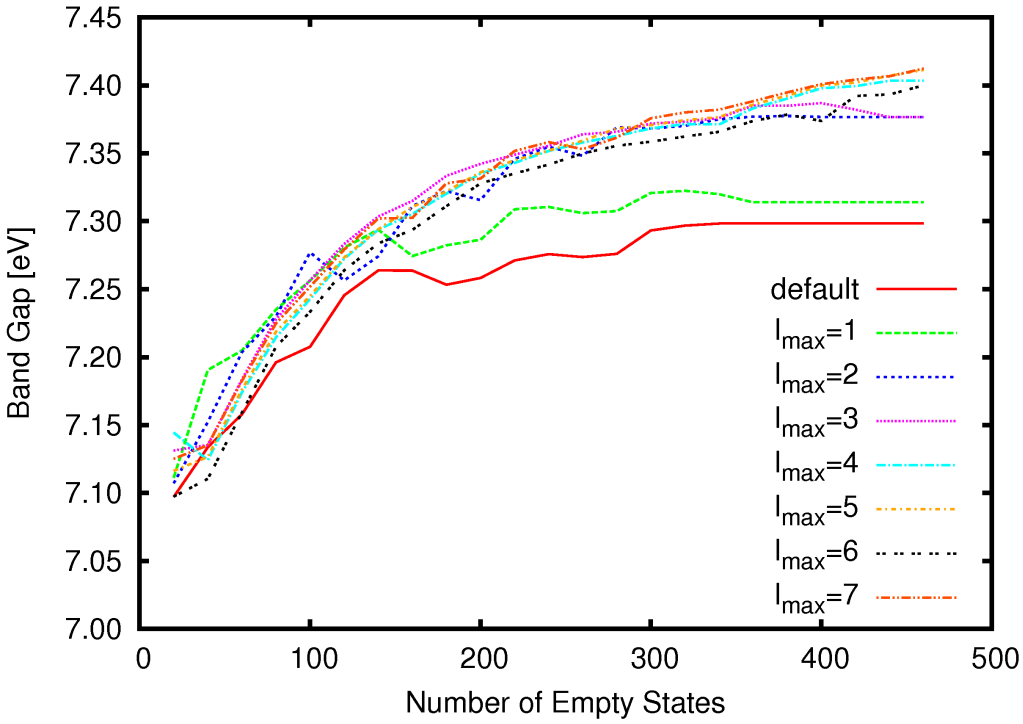

Figure 5.6: *Convergence of band gap on 2×2×2* **q***-points grid. 'default' denotes the calculation with the default description used in the* ***exciting****-code (see Chapter 2.2)*

The fact that the band-gap value is not changing for high numbers of empty states in low l-channels, especially the default description, should not be interpreted as convergence. As the number of empty states describes the number of additional eigenvalues stored and used in the calculation, an increase of the number of empty states beyond the size of the Hamiltonian matrix, which is defined by $R_{\mathrm{MT,max}} \cdot K_{max}$ and the number of local orbitals, does not change the result. As the default description yields only 351 energy eigenvalues, calculation with a higher number of empty states lead to the same results.

Figure (5.6) shows that the band gap converges with higher numbers of empty states and an that addition of local orbitals generally increases the band gap beyond the one calculated in the default basis description. The addition of local orbitals in the s,p, d and f channel give the largest contribution to this increase, further l-channels increase the band gap to a minor extent. A more detailed analysis of the convergence will follow in the next sections.

Figure (5.6) show in addition to the convergence behavior also an oscillating behavior, especially for low l_{max}. As Fig. (5.7) shows, this behavior vanishes on a finer **q**-grid. Figure(5.7) shows the the same plot as Fig. (5.6) for a 4×4×4 **q**-points grid.

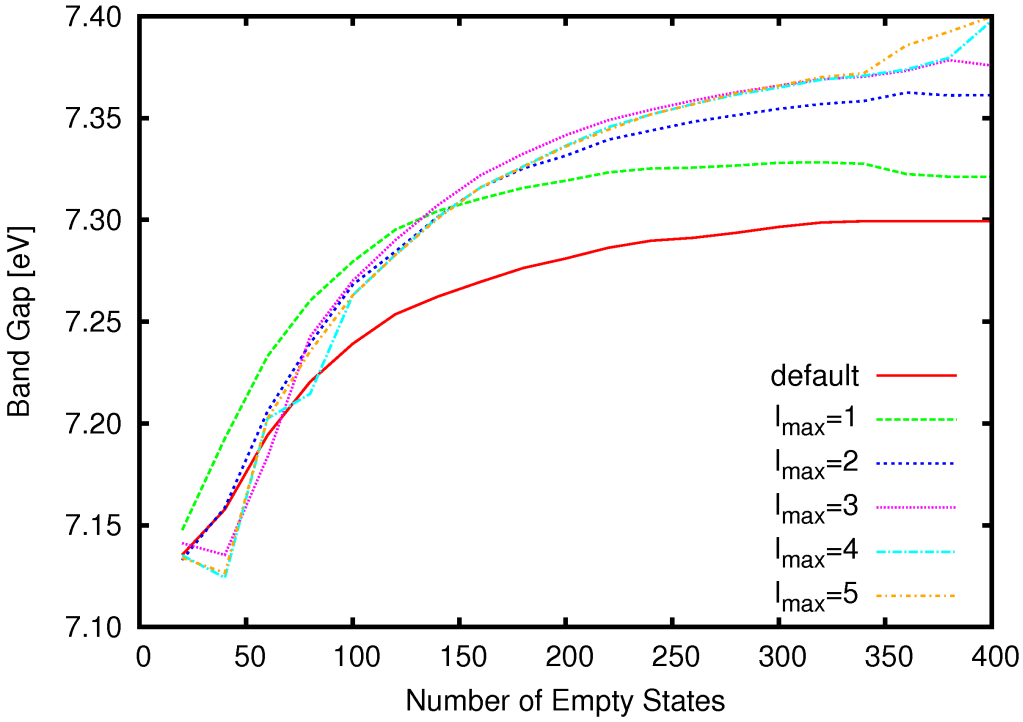

Figure 5.7: *Convergence of band gap on 4×4×4* **q***-points grid, as in figure (5.6).*

Calculations on the finer **q**-grid yield the same qualitative results already seen in Fig. (5.6), but the oscillating behavior vanishes. Calculations with $l_{max} > 3$ show an increase of the difference of band gap between calculations with high numbers of empty states beyond 350, which is one of the reasons for the complicated convergence of the band gap.

Calculations were also performed on a 6×6×6 **q**-points grid. The results of this can be seen in Fig. (5.8).

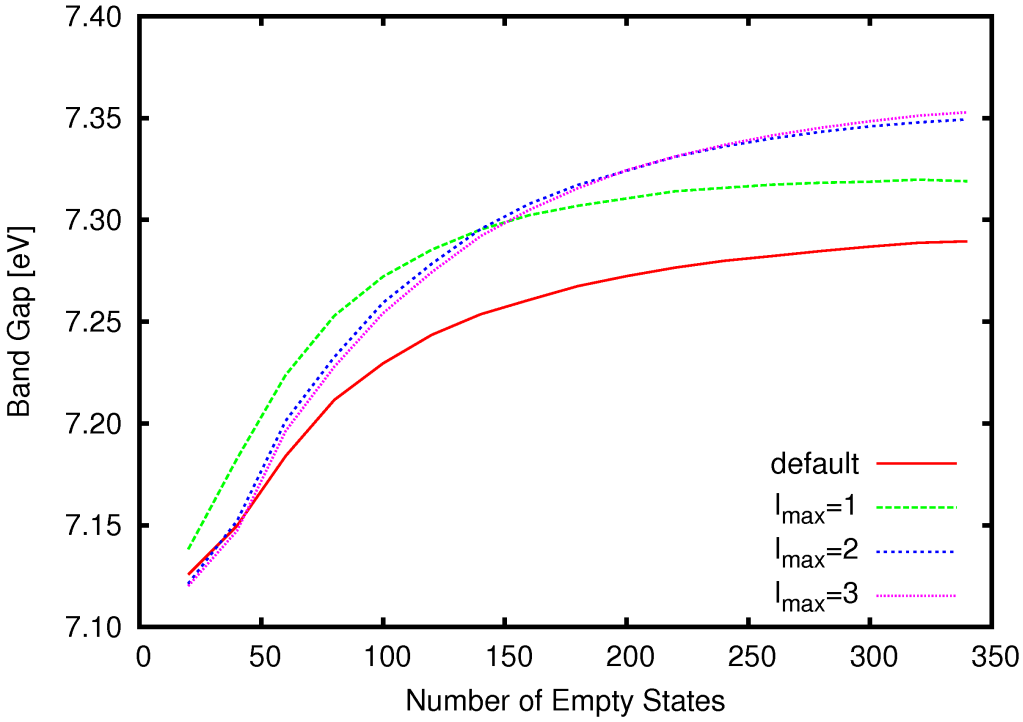

Figure 5.8: *Convergence of band gap on 6×6×6* **q***-points grid, as in figure (5.6).*

Convergence with respect to l_{max}

As the convergence of the band gap with respect to the number of empty states is slow, even for fine **q**-point grids (see Fig. (5.6), (5.7) and (5.8)) the convergence criterion is defined as

$$\left|\frac{\Delta E_g}{\Delta N_{\text{unocc}}}\right| < \frac{10\text{ meV}}{20} \tag{5.1}$$

With this criterion converged results for the band gap, depending on the l_{max}-value and the **q**-point grid, can be defined. But as the band gap is increasing with the increase of the number of empty states, band-gap results with large numbers of empty states are typically in the order of 2 to 5 meV larger than the converged results. Figure (5.9) displays the convergence of the band gap with the number of empty states on the 4×4×4 **q**-points grid. The changes in the band gap are not distributed randomly around zero but are dominantly positive, thereby increasing the band gap. If a convergence criterion is defined, the band gap calculated with many empty states is several meV higher than the 'converged' one. This behavior can be seen in Fig. (5.10). For $l_{max} > 1$ the converged and the actual band gap for the 4×4×4 **q**-points grid is higher than the ones calculated for the 4×4×4 **q**-points grid. Even for $l_{max} \geq 3$ the band gap is increased by the addition of l-channels although the addition of previos channels up to $l = 2$ gives the largest contribution in accordance with the result of the chapter above.

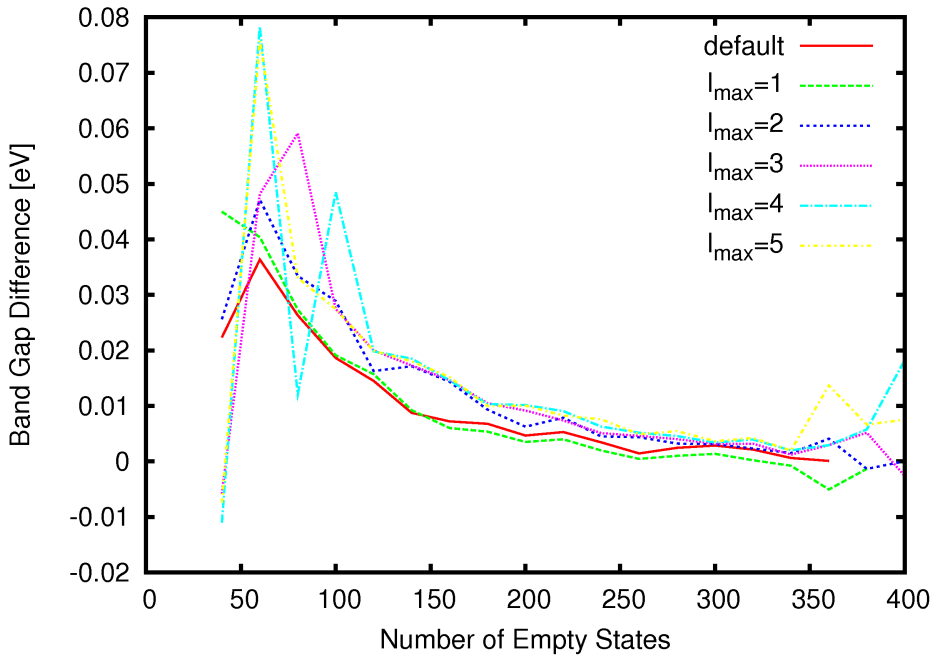

Figure 5.9: *Difference of band gap with the increase of the number of empty states for the 4×4×4* **q***-points grid*

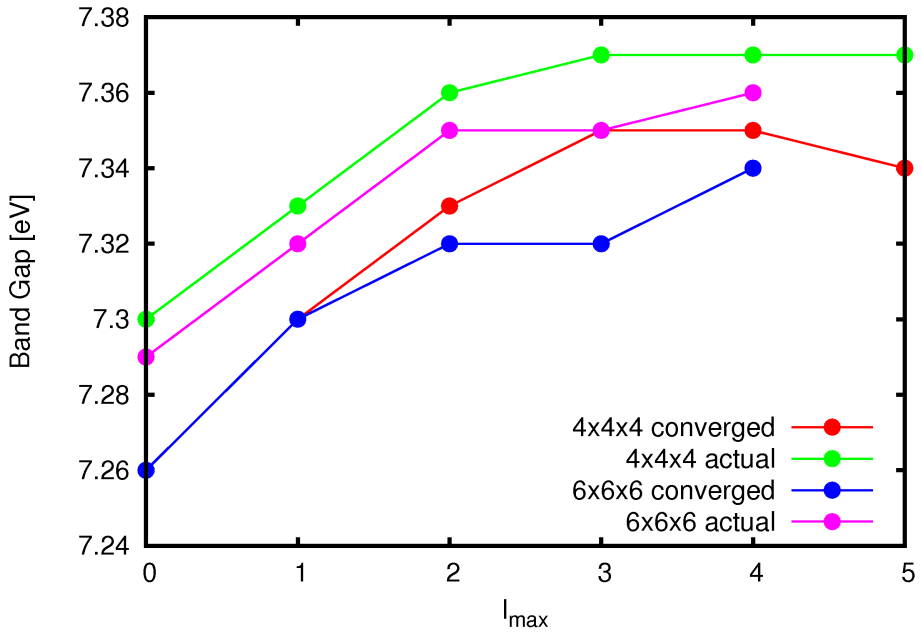

Figure 5.10: *Converged band-gap results depending on the l_{max}-value. The curves denoted 'actual' display the band gap value calculated with 340 empty states. See the text for the definition of the convergence criterion.*

For each converged band-gap result there is a corresponding number of empty states that is required to reach the convergence criterion. Figure (5.11) shows the dependence of this number of empty states on the l_{max}-value of the calculation.

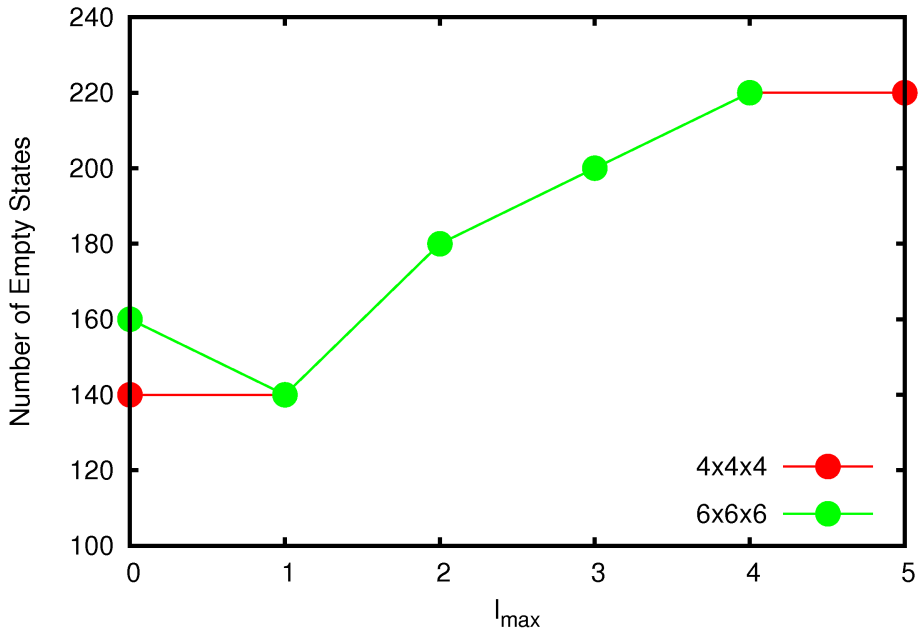

Figure 5.11: *Number of empty stated required to reach band gap convergence depending on the l_{max}-value for two different* **q***-point grids*

Figure (5.11) shows that the required number of empty states is only varying slowly. For both used **q**-point grids the required number of empty states is increasing for $1 \leq l_{max} \leq 4$. Although the addition of local orbitals changes the band-gap results it does not improve the convergence with respect to the number of empty states. On the contrary, the addition of local orbitals increases the number of empty states needed to reach the convergence criterion.

5.2.2 Analysis of Self Energy

In order to analyze the convergence of the band gap with respect to the number of unoccupied states further, the different contributions to the G_0W_0 quasiparticle energies as defined in Eq. (2.13) and their convergence with the number of unoccupied states are considered.

Self Energy Calculations

It is theoretically expected that the correlation part of the self energy depends heavily on the unoccupied states. However the exchange part is only dependent on the occupied states and therefore does not depend on the number of empty states [9, 5]. Figures (5.12) and (5.13) show the dependence of the correlation part of the self energy of the conduction band maximum and valence band minimum on the number of empty states. Calculations were performed on a 2×2×2 **q**-points grid.

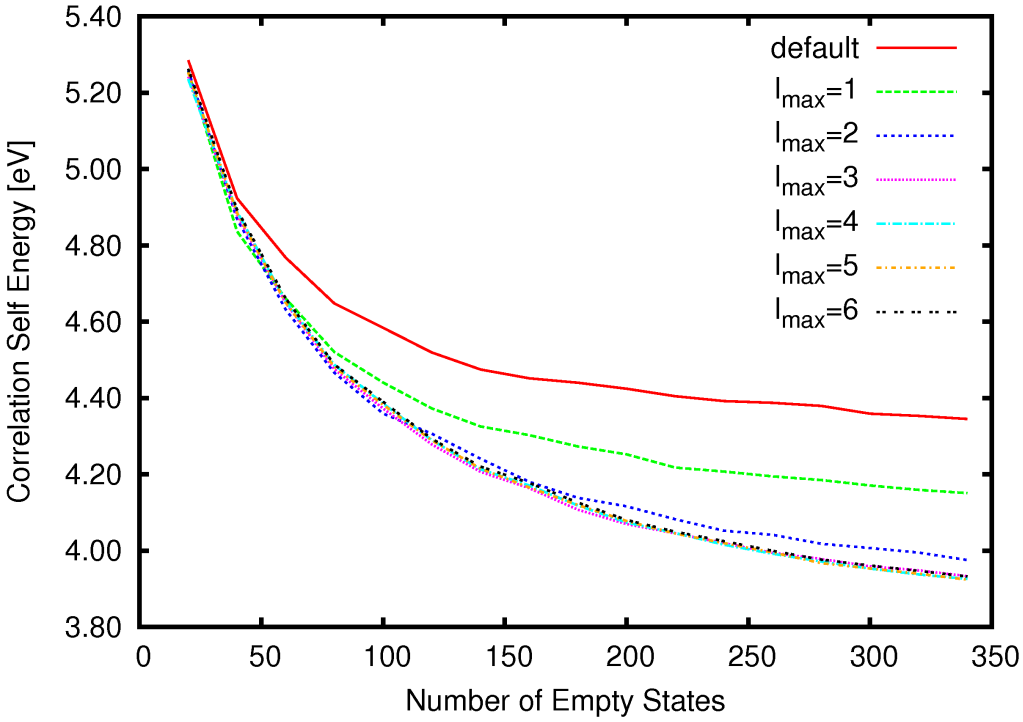

Figure 5.12: *Convergence of the correlation self energy with respect to the number of empty states for the valence band maximum using a 2×2×2* $\mathbf{q}$*-points grid*

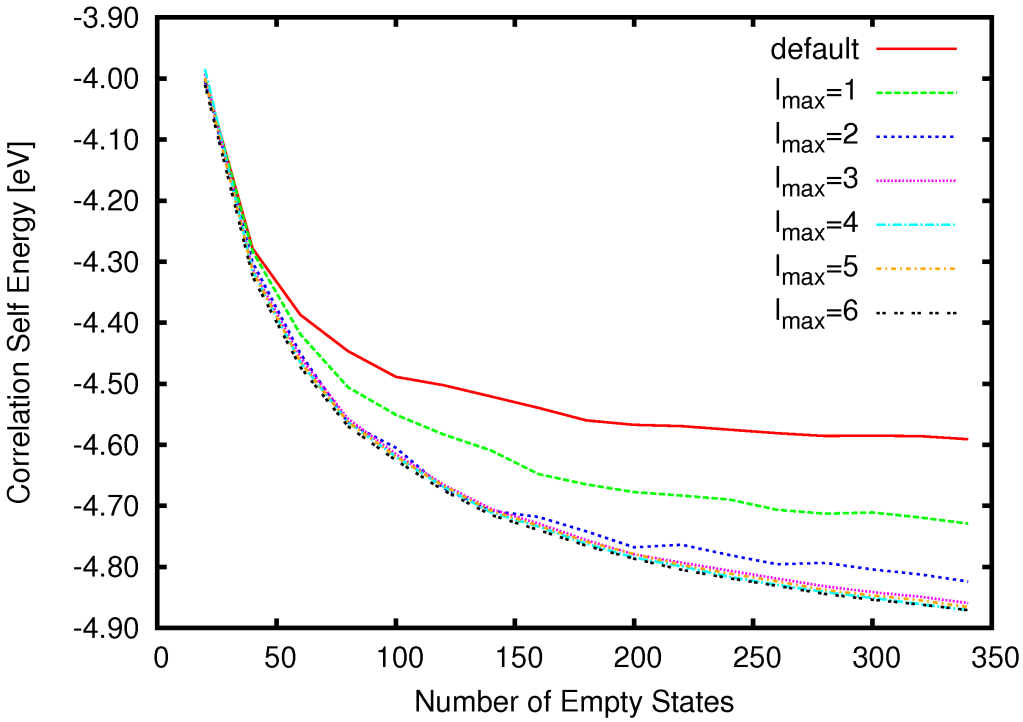

Figure 5.13: *Convergence of the correlation self energy with respect to the number of empty states for the conduction band minimum on a 2×2×2* $\mathbf{q}$*-points grid*

The rate of convergence of the exchange energy is slower than the one of the band

gap. For this reason we compare results of a calculation with a given number of empty states with those obtained by using a smaller number of empty states. As it can be seen in Fig. (5.14), that the band gap converges faster than the self energy.

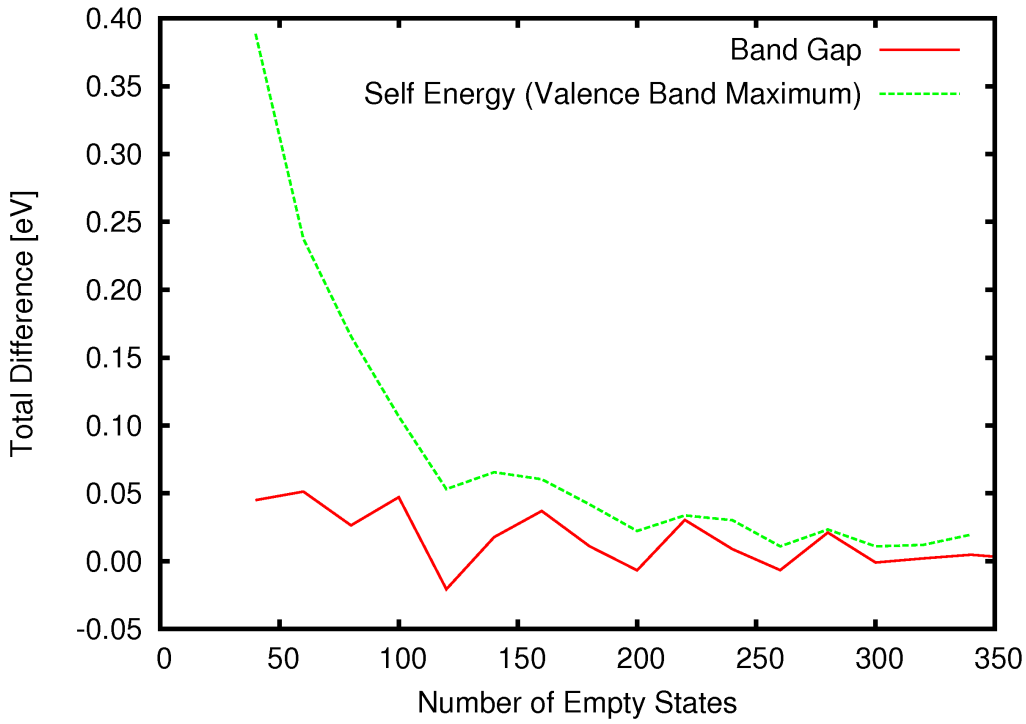

Figure 5.14: *Comparison of rate of convergence for band gap and correlation self energy on 2×2×2* **q***-points grid with* $l_{max} = 2$.

Although Fig. (5.14) displays only the behavior for $l_{max} = 2$, it is a general trend that the correlation part of the self energy for the valence band maximum as well as for the conduction band minimum converge slower than the band gap. The correlation part of the self energy is not expected depend on the number of empty states as it only depends on occupied states. As Fig. (5.15) shows, the correlation part of the self energy of the valence band maximum does not depend on the number of empty states but is dependent on the l_{max} of the used local orbitals. It is increasing if local orbitals with $l_{max} = 1$ and $l_{max} = 2$ are added, a further addition of local orbitals does not change the self energy.

As occupied states have description dominated by the radial functions with low l-character up to d-character, local orbitals in the low l-channels change the description of this states. Local orbitals in higher l-channels do not contribute due to the orthogonality of the radial functions in different l-channels.

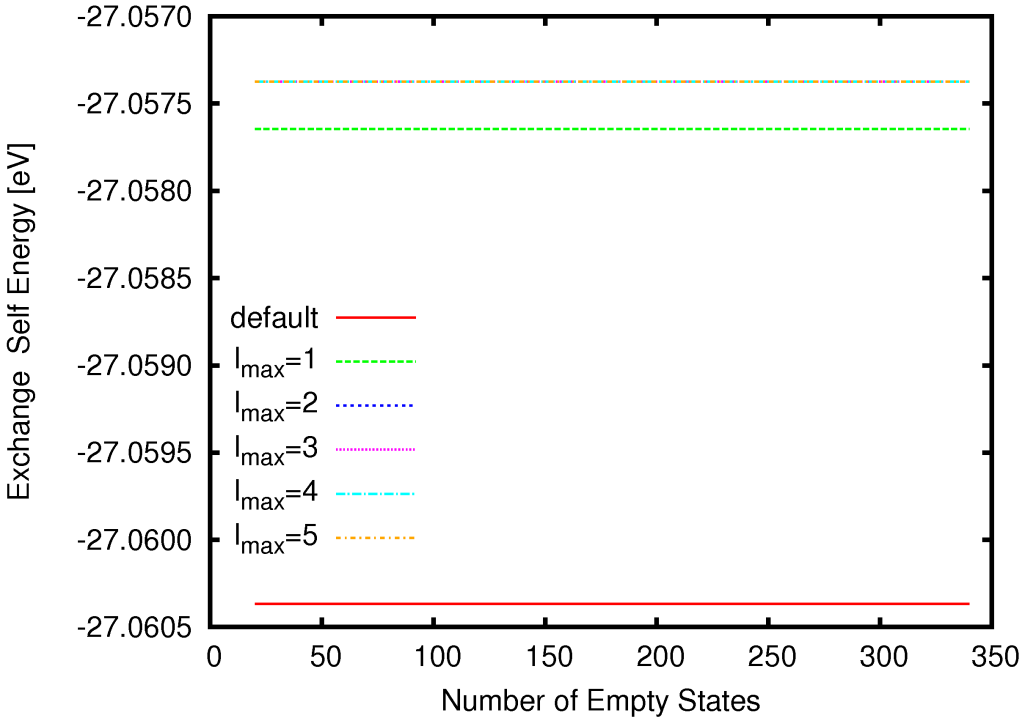

Figure 5.15: *Dependence of the exchange self energy on the number of empty states on 2×2×2* **q***-points grid. Displayed is the exchange part of the self energy for the valence band maximum.*

It can also be seen that the changes in the exchange part of the self energy are negligible in comparison to the changes in the correlation part of the self energy, especially if calculations with different numbers of empty states are performed.

Chapter 6

Conclusion

Unoccupied States in Groundstate Calculations

A systematic scheme for the inclusion of local orbitals in the high-energy region is proposed which is based on two parameters. The parameter l_{max} and E_c determine the maximal l-channel used for local orbitals and the highest reference energy at which local orbitals are set. Basis set completeness can be analyzed in this scheme in terms of the convergence of the density of states with respect to E_c and l_{max}. It is shown that a convergence criterion of $\Delta_{TDOS} = \pm 0.2$ Ha^{-1}a$_0{}^{-3}$ for the density of states yields differences in the energy eigenvalues at the Γ-point of less than 0.3 eV, reflecting that the density of states is an appropriate property to evaluate basis set convergence in the unoccupied energy region.

The converged energy region increases linearly with l_{max}. s,p and d local orbitals are only sufficient to reach convergence for a few Ha above the Fermi energy. In order to achieve basis set completeness in the high energy region, the inclusion in high l-channels is necessary.

Unoccupied States in G_0W_0-calculations

The band gap increases with the addition of local orbitals, the biggest contribution arise from local orbitals in the s, p and d channel. This convergence of the band gap is due to the convergence of the correlation part of the self energy.

The convergence of the band gap with respect to the number of empty states turns out to be slow in the case of MgO and local orbitals do not improve the convergence. The number of empty states required to reach a convergence criterion of ± 0.01 eV for the band gap slightly increases with l_{max}. This indicates that the slow convergence with respect to the number of empty states is not caused by the linearization error of high lying states.

Evaluating the convergence of the band gap with respect to l_{max} on different $\mathbf{q}$-point grids yield a converged result for the band gap E_g^{GW}. Although contributions of local orbitals in high l-channels are small, it is found to be necessary to include local orbitals with $l_{max} = 5$. Table (6.1) compares the band gap to the experimental one E_g^{exp} and the one calculated with DFT using the PBEsol functional E_g^{PBEsol}:

E_g^{GW}	E_g^{exp} [11]	E_g^{PBEsol}
7.34 ev	7.83 eV	4.74 eV

Table 6.1: Converged G_0W_0 band-gap result E_g^{GW} compared to experimental value E_g^{exp} and DFT result E_g^{PBEsol}

Acknowledgment

This Bachelor Thesis would not have been possible without the support of Prof. Dr. Dr. hc Draxl, Dr. Nabok, Dr. Pavone and the whole working group.
I also want to thank my parents for supporting me the last three years and all the time before.

Appendix

Convergence with respect to l_{max}^{MB}

In the G_0W_0 approximation, in addition to the KS-wavefunction also products of two wavefunctions are used. The `exciting` code uses a separate basis, the so called mixed basis, to calculate products of wavefunctions. Details of the theoretical background and implementation of this basis can be found in Ref. [9] and references therein.

A central parameter in the mixed basis is l_{max}^{MB}. Within the muffin-tin sphere only the products of radial functions u_l and $u_{l'}$ which obey the in equation

$$|l - l'| \leq l_{max}^{\mathrm{MB}} \leq l + l' \tag{1}$$

are taken into account. Products of radial functions and the derivatives $\dot{u}_l$ are not used to form the mixed basis.

A convergence test was performed to evaluate the influence of this mixing parameter on the convergence of the band gap with respect to the number of empty states. The results are shown in Fig. (1).

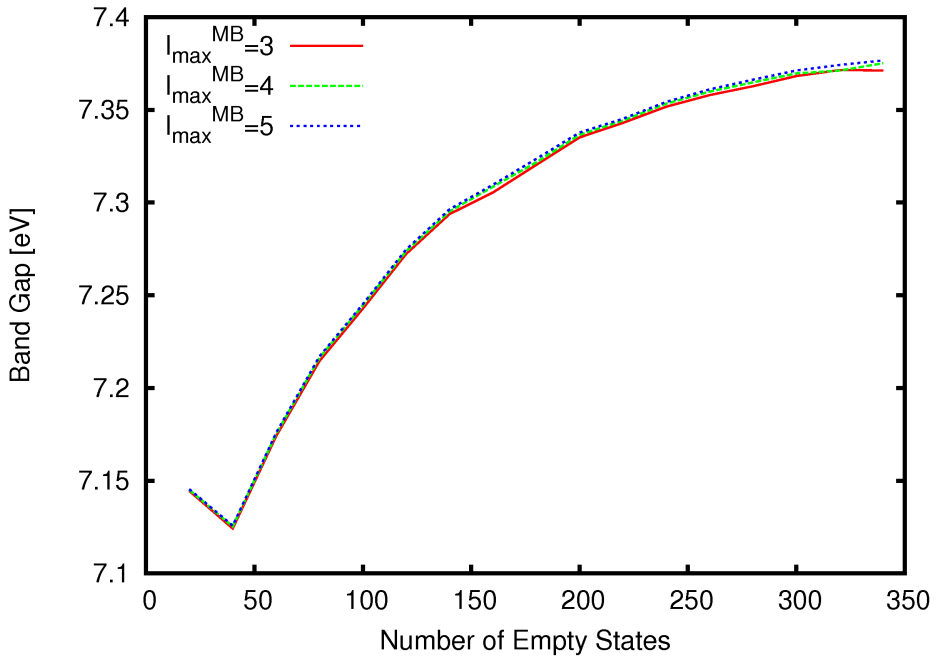

Figure 1: *Influence of the parameter l_{max}^{MB} on the band gap for $l_{max} = 4$ and a 2×2×2* **q***-points grid*

Increasing the parameter beyond the default value of 3 does not change the band gap significantly. As local orbitals are added in all l-channels up to l_{max} already a small mixing parameter ensures that a sufficient amount of local orbitals in high l-channels is included in the G_0W_0 calculation.

Convergence with respect to K_{max}

To evaluate the influence of K_{max} on the band-gap calculations, groundstate calculations with different K_{max} and $l_{max} = 2$ as basis for G_0W_0 calculations for a 4×4×4 **q**-points grid were performed. The band gap is increasing with an increase of K_{max} and because the size of the plane-wave basis is defined by this parameter. Calculations with low K_{max} have less unoccupied states. This is the reason why for high numbers of empty states the band gap does not longer depend on the number of empty states. Results are displayed in Fig. (2).

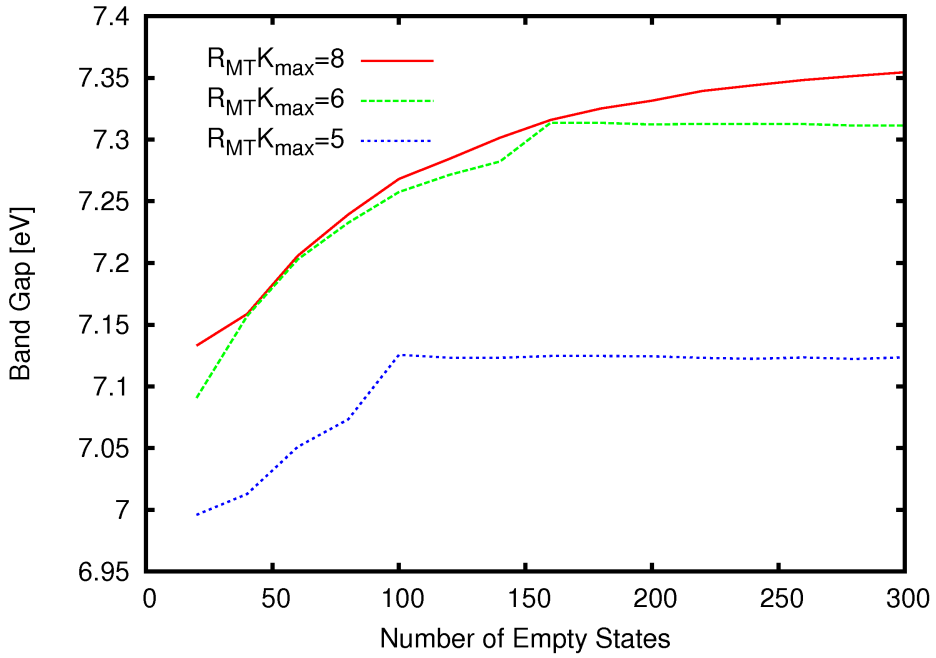

Figure 2: *Influence of the parameter K_{max} on the band gap for $l_{max} = 2$ and a 4×4×4* **q***-points grid*

Bibliography

[1] Ambrosch-Draxl, C: Augmented Planewave Methods. In: *Phys. Scr.* T109 (2004), 48-53. http://stacks.iop.org/1402-4896/T109/48

[2] Ambrosch-Draxl, C. ; Sagmeister, S. ; Meisenbichler, Ch. ; Spitaler, J.: *exciting code*. [online] http://exciting-code.org, 2009

[3] Burke, K.: Perspective on density functional theory. In: *J. Chem. Phys.* 136 (2012), 150901. http://link.aip.org/link/doi/10.1063/1.4704546

[4] Friedrich, Christoph ; Müller, Mathias C. ; Blügel, Stefan: Band convergence and linearization error correction of all-electron *GW* calculations: The extreme case of zinc oxide. In: *Phys. Rev. B* 83 (2011), Feb, 081101. http://dx.doi.org/10.1103/PhysRevB.83.081101. – DOI 10.1103/PhysRevB.83.081101

[5] Friedrich, Christoph ; Schindlmayr, Arno ; Blügel, Stefan ; Kotani, Takao: Elimination of the linearization error in *GW* calculations based on the linearized augmented-plane-wave method. In: *Phys. Rev. B* 74 (2006), Jul, 045104. http://dx.doi.org/10.1103/PhysRevB.74.045104. – DOI 10.1103/PhysRevB.74.045104

[6] Hedin, Lars ; Lundqvist, Stig: Effects of Electron-Electron and Electron-Phonon Interactions on the One-Electron States of Solids. Version: 1970. http://dx.doi.org/10.1016/S0081-1947(08)60615-3. Academic Press, 1970. – DOI 10.1016/S0081–1947(08)60615–3. – ISSN 0081–1947, 1 - 181

[7] Hohenberg, P. ; Kohn, W.: Inhomogeneous Electron Gas. In: *Phys. Rev.* 136 (1964), Nov, B864–B871. http://dx.doi.org/10.1103/PhysRev.136.B864. – DOI 10.1103/PhysRev.136.B864

[8] Hybertsen, Mark S. ; Louie, Steven G.: Electron correlation in semiconductors and insulators: Band gaps and quasiparticle energies. In: *Phys. Rev. B* 34 (1986), Oct, 5390–5413. http://dx.doi.org/10.1103/PhysRevB.34.5390. – DOI 10.1103/PhysRevB.34.5390

[9] Jiang, Hong ; Gomez-Abal, Ricardo I. ; Li, Xin-Zheng ; Meisenbichler, Christian ; Ambrosch-Draxl, Claudia ; Scheffler, Matthias: FHI-gap: A code based on the all-electron augmented plane wave method. In: *Computer Physics Communications* 184 (2013), Nr. 2, 348 - 366. http://dx.doi.org/10.1016/j.cpc.2012.09.018. – DOI 10.1016/j.cpc.2012.09.018. – ISSN 0010–4655

[10] Kohn, W. ; Sham, L. J.: Self-Consistent Equations Including Exchange and Correlation Effects. In: *Phys. Rev.* 140 (1965), Nov, A1133–A1138. http://dx.doi.org/10.1103/PhysRev.140.A1133. – DOI 10.1103/PhysRev.140.A1133

[11] Oganov, Artem R. ; Gillan, Michael J. ; Price, G. D.: Ab initio lattice dynamics and structural stability of MgO. In: *The Journal of Chemical Physics* 118 (2003), Nr. 22, 10174-10182. http://dx.doi.org/10.1063/1.1570394. – DOI 10.1063/1.1570394

[12] Perdew, J. P. ; Burke, K. ; Ernzerhof, M.: Generalized Gradient Approximation Made Simple. In: *Phys. Rev. Lett.* 77 (1996), S. 3865

[13] Singh, David: Ground-state properties of lanthanum: Treatment of extended-core states. In: *Phys. Rev. B* 43 (1991), Mar, 6388–6392. http://dx.doi.org/10.1103/PhysRevB.43.6388. – DOI 10.1103/PhysRevB.43.6388

[14] Singh, David J.: *Planewaves, Pseudopotentials, and the LAPW Method*. Boston : Kluwer, 1994

[15] Sjoestedt, E ; Nordstroem, L ; Singh, D.J: An alternative way of linearizing the augmented plane-wave method. In: *Solid State Communications* 114 (2000), Nr. 1, 15 - 20. http://dx.doi.org/10.1016/S0038-1098(99)00577-3. – DOI 10.1016/S0038–1098(99)00577–3. – ISSN 0038–1098

[16] Slater, J. C.: Wave Functions in a Periodic Potential. In: *Phys. Rev.* 51 (1937), S. 846

Selbständigkeitserklärung

Hiermit erkläre ich, dass ich die Arbeit selbständig verfasst und keine anderen als die angegebenen Quellen und Hilfsmittel verwendet habe.

Berlin, der 30. Juni 2013

Christian Vorwerk